

RESEARCH ARTICLE

Mitochondrial NCKX5 regulates melanosomal biogenesis and pigment production

Zhao Zhang^{1,2,3}, Juanjuan Gong², Elena V. Sviderskaya⁴, Aihua Wei^{5,*} and Wei Li^{2,6,*}

ABSTRACT

Oculocutaneous albinism (OCA) is a heterogeneous and autosomal recessive hypopigmentation disorder, which is caused by mutations of genes involved in pigment biosynthesis or melanosome biogenesis. We have previously identified *NCKX5* (also known as *SLC24A5*) as a causative gene for OCA type 6 (OCA6). However, the pathogenesis of OCA6 is unknown. We found that *NCKX5* is localized to mitochondria, not to melanosomes. Pharmacological inhibition of mitochondrial function or *NCKX* exchanger activity reduced pigment production. Loss of *NCKX5* attenuated Ca^{2+} enrichment in melanosomes, which compromised PMEL fibril formation, melanosome maturation and pigment production. Thus, we have defined a new class of hypopigmentation attributable to dysfunctional mitochondria and an impairment of mitochondrial Ca^{2+} transfer into melanosomes. Thus, it is possible that mitochondrial function could have a role in the graying of hair in older people and formation of hypopigmented lesions in vitiligo patients.

KEY WORDS: Melanosome, Mitochondrion, NCKX5, SLC24A5, Oculocutaneous albinism, Pigment

INTRODUCTION

Albinism is a rare inherited disease characterized by poor vision and variable hypopigmentation manifestations. The absence or reduction in pigment occurs in the skin, hair and eyes (oculocutaneous albinism, OCA) or mainly in the eyes (ocular albinism, OA) (Li et al., 2006). At least 18 genes have been identified as causative genes for human albinism. These include six nonsyndromic OCA genes (type of OCA is given in brackets), *TYR* (OCA1), *OCA2* (OCA2), *TYRP1* (OCA3), *SLC45A2* (OCA4), *SLC24A5* (OCA6), *C10ORF11* (OCA7), and one single gene associated with OA, *GPRI43* (OA1). Moreover, there are an additional eleven syndromic OCA genes, including ten Hermansky–Pudlak syndrome (HPS) genes (type of HPS is given in brackets), *HPS1* (HPS1), *AP3B1* (HPS2), *HPS3* (HPS3), *HPS4* (HPS4), *HPS5* (HPS5), *HPS6* (HPS6), *DTNBPI* (HPS7), *BLOC1S3* (HPS8), *BLOC1S6* (HPS9), *AP3D1* (HPS10),

and one Chediak–Higashi syndrome (CHS) gene, *LYST* (also known as *CHSI*) (Ammann et al., 2016; Li et al., 2006; Wei and Li, 2013).

Currently, OCA is categorized into two groups. One group involves the lack of melanosomal proteins, such as tyrosinase, OCA2 or TYRP1 which leads to non-syndromic OCA1–OCA3 subtypes, respectively. The other group involves a deficiency of melanosomal transporting complexes, such as HPS protein-associated complexes (HPACs), which lead to the defective melanosomes seen in HPS. Syndromic OCA is often accompanied by disrupted biogenesis of a group of lysosome-related organelles (LROs), including melanosomes in melanocytes, dense granules in platelets and lamellar bodies in lung type 2 epithelial cells, and patients can exhibit additional symptoms such as prolonged bleeding and fatal lung disease in some cases (Wei and Li, 2013). We previously adopted whole-exome sequencing with a family-based recessive mutation model, and newly identified *SLC24A5* as a defined causative gene for a nonsyndromic type of OCA, which has been designated as OCA6 (Wei et al., 2013). The human *SLC24A5* gene, encodes a member of the K^{+} -dependent $\text{Na}^{+}/\text{Ca}^{2+}$ exchanger family, *NCKX5* (Lamason et al., 2005). Endogenous human *NCKX5* is partially localized to the trans-Golgi network (TGN) (Ginger et al., 2008). Proteomics analysis has revealed that *NCKX5* is present in melanosomes (Chi et al., 2006), suggesting it is a melanosomal protein (Ito and Wakamatsu, 2011). However, the precise melanosomal localization of *NCKX5* in melanocytes is not known and it is unclear whether *NCKX5* is a melanosomal protein or is associated with any melanosomal transporting complexes. Thus, the group of OCA that OCA6 falls in remains unsettled.

Melanosomes can be morphologically classified into four distinct stages (I–IV) based on the degree of maturation (Sitaram and Marks, 2012). Melanosomes originate from recycling endosomes (Raposo et al., 2001). The melanosomal scaffolding protein PMEL is a driving force for premelanosome fibril formation (Berson et al., 2001; Kushimoto et al., 2001; Raposo et al., 2001). Processing of PMEL is mediated by a furin-like protease, whose activity is highly Ca^{2+} dependent (Thomas, 2002). However, the origin of melanosomal Ca^{2+} is unknown. Several organelles such as the ER, mitochondria and lysosomes are highly enriched with Ca^{2+} . The ER is believed to be the major intracellular Ca^{2+} pool for supplying Ca^{2+} to other organelles (Burgoyne et al., 2015). Domains between the ER and mitochondria called mitochondria-associated membranes (MAMs) (Vance, 1990), selectively mediate the transfer of Ca^{2+} from the ER to mitochondria (Rizzuto et al., 2009, 1998). Melanosomes are acidic organelles containing high Ca^{2+} levels (Bush and Simon, 2007; Hoogdijn et al., 2003; Patel and Docampo, 2010). The melanosome is a type of LROs (Wei and Li, 2013). Likewise, lysosomes and other acidic LROs similarly store Ca^{2+} (Patel and Docampo, 2010). It was recently reported that lysosomal Ca^{2+} originates from the ER (Garrity et al., 2016). However, the source of Ca^{2+} for LROs remains uncertain. LRO Ca^{2+} is thought to originate either from organelle contacts with the ER or from cytosol

¹State Key Laboratory of Molecular Developmental Biology, Institute of Genetics and Developmental Biology, Chinese Academy of Sciences, Beijing 100101, China. ²Beijing Key Laboratory for Genetics of Birth Defects, Beijing Pediatric Research Institute; MOE Key Laboratory of Major Diseases in Children; Genetics and Birth Defects Control Center, National Center for Children's Health; Beijing Children's Hospital, Capital Medical University, Beijing 100045, China. ³University of Chinese Academy of Sciences, Beijing 100039, China. ⁴Cell Signalling Research Centre, St. George's, University of London, London SW17 0RE, UK. ⁵Department of Dermatology, Beijing Tongren Hospital, Capital Medical University, Beijing 100730, China. ⁶Shunyi Women and Children's Hospital of Beijing Children's Hospital, Beijing 101300, China.

*Authors for correspondence (liweili@bch.com.cn; weiaihua3000@163.com)

© Z.Z., 0000-0002-5086-5278; J.G., 0000-0003-2190-2954; A.W., 0000-0003-3381-4230; W.L., 0000-0001-7430-6019

and be transferred by Ca^{2+} transporters, driven by ATP hydrolysis (Patel and Docampo, 2010). In fact, cytosolic Ca^{2+} is relatively low in resting conditions (Berridge et al., 2000). Ca^{2+} in the ER or other Ca^{2+} -enriched organelles could be transferred to LROs through physical contacts with these organelles. The connections between mitochondria and melanosomes are morphologically similar to the ER–mitochondria contacts, and are also modulated by a fusion player MFN2 (Daniele et al., 2014). We therefore hypothesize that melanosome–mitochondria contact sites may serve as exchanging sites for Ca^{2+} .

There are two families of $\text{Na}^+/\text{Ca}^{2+}$ exchangers, the K^+ -independent $\text{Na}^+/\text{Ca}^{2+}$ exchanger family (NCX) and the K^+ -dependent $\text{Na}^+/\text{Ca}^{2+}$ exchanger family (NCKX) (Blaustein and Lederer, 1999). NCKX5 possesses NCKX activity in a heterologous expression system (Ginger et al., 2008). In this study, we found that NCKX5 is enriched in mitochondria, and we further defined that mitochondrial NCKX5 plays an important role in regulating the melanosomal Ca^{2+} homeostasis that is required for melanosome maturation and pigment production, which explains the pathogenesis of OCA6.

RESULTS

NCKX5 is localized to mitochondria and the TGN, but not to melanosomes

As the precise subcellular localization of NCKX5 is controversial, we sought to determine the exact subcellular localization of NCKX5 in melanocytes. A full-length mouse *Nckx5* transgene with a Myc epitope tag inserted in-frame into the protein (NCKX5–Myc) was generated. When expressed in melan-a melanocytes, NCKX5–Myc did not colocalize with PMEL (an immature melanosomal marker) (Fig. 1A) or TYRP1 (a mature melanosomal marker) (Fig. 1B). In addition, NCKX5–Myc did not colocalize with pigment granules as visualized by bright-field microscopy (Fig. 1C). However, we observed partial colabeling of NCKX5–Myc with the trans-Golgi network (TGN) marker TGN38 (also known as TGOLN2) (Fig. 1D), confirming that NCKX5 is partially localized to the TGN (Ginger et al., 2008). To our surprise, transiently transfected NCKX5–Myc largely colocalized with the mitochondrial marker cytochrome *c* (Fig. 1E). To confirm this result, we detected endogenous NCKX5 localization by labeling the melan-a melanocytes with three different anti-NCKX5 polyclonal antisera (Fig. 1F). Consistent with the results with overexpressed NCKX5–Myc, the endogenous NCKX5 colocalized with mitochondrial protein cytochrome *c* as well (Fig. 1G–I). In almost all observed melan-a melanocytes, the endogenous NCKX5 detected by NCKX5–C4 polyclonal antisera exhibited a mitochondrial distribution pattern (Fig. 1J,K). However, in some melanocytes (~30%) the overexpressed NCKX5–Myc did not localize to mitochondria, only localizing at the perinuclear area with a TGN distributional pattern (Fig. 1L–N). Nevertheless, our immunofluorescence microscopy (IFM) results suggest that NCKX5 is localized to mitochondria and the TGN, but not to melanosomes in melan-a melanocytes.

Disruption of NCKX5 compromises melanosomal Ca^{2+} concentration, melanosomal PMEL expression and melanin production

We next investigated how NCKX5 functions in pigment production in melanocytes. Western blot analysis showed that melan-a melanocytes treated with NCKX5-specific siRNA (NCKX5-KD) dramatically decreased the expression of NCKX5 (Fig. 2A). Consequently, melanin production was greatly reduced in NCKX5-KD (knockdown) melanocytes, which was restored by

expressing exogenous NCKX5–Myc (Fig. 2B), but not by the reported mutants NCKX5-L454Ffs31X–Myc and NCKX5-S182R–Myc (Morice-Picard et al., 2014; Wei et al., 2013; data not shown), confirming the reduced pigmentation seen in the OCA6 patient with loss of NCKX5 (Wei et al., 2013).

NCKX5 has $\text{Na}^+/\text{Ca}^{2+}$ exchanger activity in a heterologous expression system (Ginger et al., 2008). We therefore reasoned that NCKX5 could affect melanosomal Ca^{2+} homeostasis in some way. To detect melanosomal Ca^{2+} , we engineered a construct with that fused the genetically modified Ca^{2+} sensor GCaMP6 to the N-terminus of tyrosinase (TYR), which is expressed on the luminal side of the melanosome membrane. Indeed, NCKX5-KD cells exhibited a reduced level of GCaMP6 fluorescence intensity, indicative of lower luminal melanosomal Ca^{2+} concentration compared with that seen in control (Ctrl) cells (Fig. 2C,D).

Melanosomal scaffolding protein PMEL is cleaved by a furin-like protease to form PMEL fibrils, in a process that is strictly Ca^{2+} dependent (Berson et al., 2003; Thomas, 2002). We speculate that reduced melanosomal Ca^{2+} level may disrupt PMEL processing. The monoclonal antibody HMB45, which specifically recognizes the luminal fragment of PMEL (Hoashi et al., 2006; Yasumoto et al., 2004), is used for monitoring fibrillar formation of PMEL, a critical step in melanosome biogenesis. IFM analysis showed that PMEL puncta were observed in control cells, but were invisible in NCKX5-KD cells (Fig. 2E). In addition, fibril-enriched detergent-insoluble PMEL was not detectable in NCKX5-KD cells in an immunoblotting assay (Fig. 2G). These results are consistent with the hypothesis that disruption of PMEL sorting and processing leads to the degradation of PMEL luminal domain together with the transmembrane fragment (Niel et al., 2011), confirming the reduction of mature melanosomes seen in the skin melanocytes of the OCA6 patient (Wei et al., 2013).

There are two families of $\text{Na}^+/\text{Ca}^{2+}$ exchangers, the NCX and NCKX family (Blaustein and Lederer, 1999). The NCKX family consists of five members. While the NCKX1–NCKX4 proteins are mainly localized to the plasma membrane (Schnetkamp, 2013), NCKX5 is localized to mitochondria and TGN in melanocytes (as shown in Fig. 1). However, it has been reported that Ca^{2+} efflux from mitochondria is mediated by another $\text{Na}^+/\text{Ca}^{2+}$ exchanger, NCLX (also known as SLC8B1), a member of the NCX family (Luongo et al., 2017; Palty et al., 2010). We therefore tested whether NCLX or NCKX activity is required for melanogenesis. We treated cells with the NCKX inhibitor DBZ (Altimimi et al., 2013; Shumilina et al., 2010) and the NCX inhibitor CGP-37157 (Cox et al., 1993; Palty et al., 2010). IFM analysis showed that the number of PMEL puncta was decreased upon DBZ treatment, but was less affected by CGP-37157 treatment (Fig. 2F). Immunoblotting assays revealed that the intensity of low molecular mass band of PMEL was specifically decreased, and the high molecular mass band of PMEL was apparently increased by DBZ treatment but not by CGP-37157 treatment (Fig. 2G), suggesting that disruption of NCKX but not NCX activity compromises proteolytic processing of PMEL, thereby leading to an accumulation of its precursor. Taken together, these results suggest that NCKX5 possesses the NCKX activity that plays a key role in regulating melanosomal Ca^{2+} homeostasis and thus regulates PMEL processing, melanosome maturation and pigment production.

The Ca^{2+} indicators Rhod-2 and X-Rhod-1 show efflux from mitochondria and influx into melanosomes in a time-dependent manner

Previous findings have shown physical contacts between mitochondria and melanosomes (Daniele et al., 2014). These

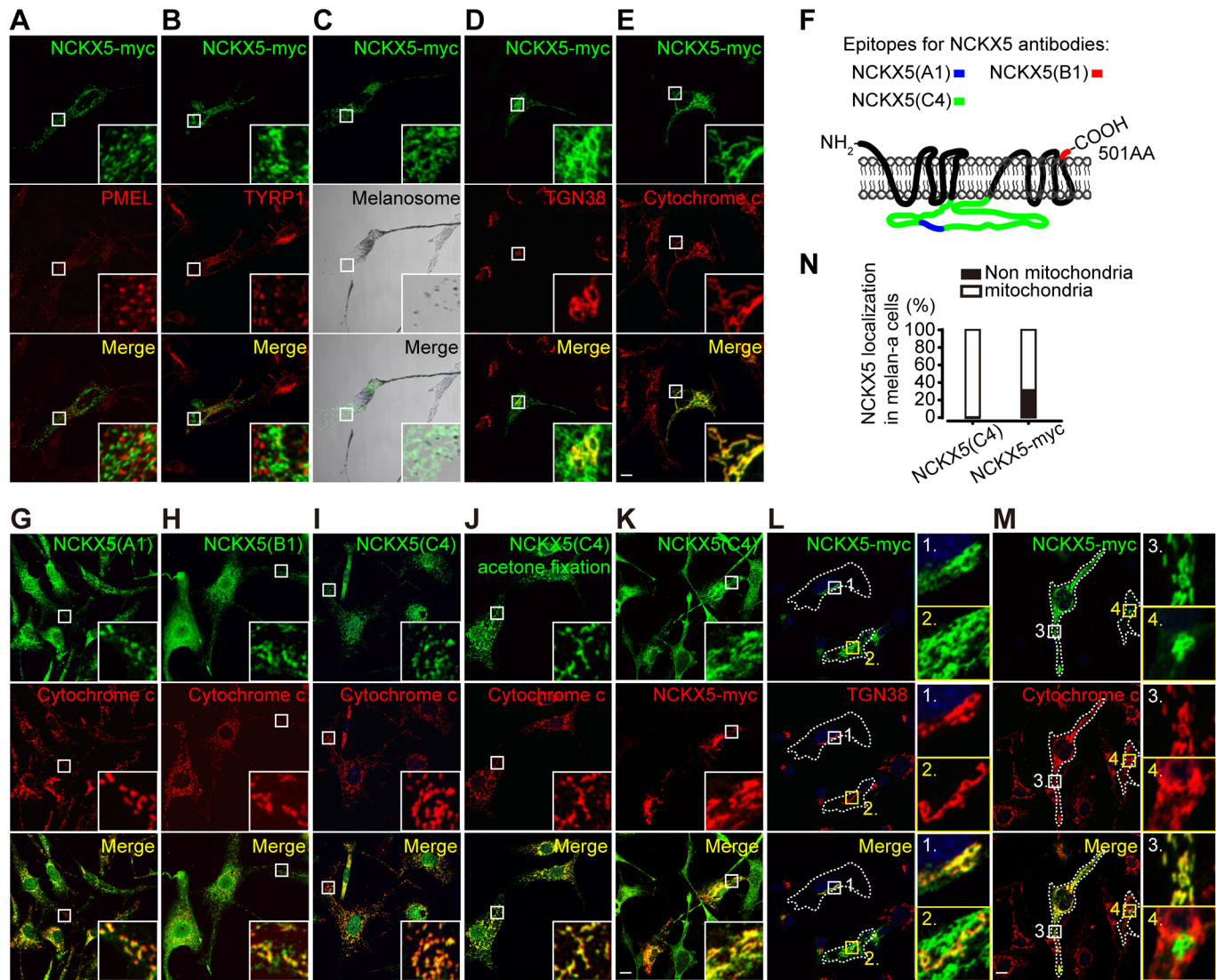


Fig. 1. NCKX5 is predominantly localized to mitochondria. (A–E) Melan-a melanocytes were transfected with the NCKX5–Myc transgene and incubated with antibodies against PMEL (A), TYRP1 (B), TGN38 (D) and cytochrome *c* (E). BF images of pigmented melanosomes were also acquired (C). Insets show 5× magnified images of the boxed region. (F) Schematic of the peptides used to generate NCKX5 polyclonal anti-sera. (G–J) Melan-a melanocytes were colabeled with NCKX5 polyclonal anti-sera [NCKX5(A1) in G; NCKX5(B1) in H; NCKX5(C4) in I and J (J shows images after acetone fixation)] and antibody against cytochrome *c*. Insets show 5× magnified images of the boxed region. (K) Melan-a melanocytes were transfected with the NCKX5–Myc transgene and colabeled with NCKX5 polyclonal anti-sera. (L, M) Melan-a melanocytes were transfected with the NCKX5–Myc transgene and incubated with antibodies for a marker of the TGN (L, TGN38) or cytochrome *c* (M). Outlines of cells are indicated by dashed white lines. Insets show 6× magnified images of the boxed region. (N) The percentage of the NCKX5 [anti-NCKX5(C4) and -NCKX5–Myc] colocalized with cytochrome *c*; $n=265$ and 88 melanocytes, respectively. Scale bars: 10 μm .

contacts are morphologically similar to ER–mitochondria tethers, which may be the locations at which selective transfer of Ca^{2+} from ER to mitochondria occurs (Rizzuto et al., 2009; Rizzuto et al., 1998). As NCKX5 is enriched in mitochondria (Fig. 1) and regulates the melanosomal Ca^{2+} level (Fig. 2C,D), we speculated that mitochondrial Ca^{2+} might be transferred to melanosomes in a similar manner. It is hard to trace the flow of free Ca^{2+} ions between organelles. Hence, we monitored this exchange by an indirect method. Rhodamine-2/acetoxymethyl ester (Rhod-2/AM) is a widely used Ca^{2+} tracer. Esterolysis of the permeant cation Rhod-2/AM generates zwitterionic Rhod-2, which is trapped in mitochondria (Minta et al., 1989), and represents mitochondrial Ca^{2+} (Fonteriz et al., 2010; Kostic et al., 2015; Palty et al., 2010). Cells transfected with construct encoding a mitochondrially located GFP (mito-GFP) were incubated with Rhod-2/AM for 30 min for

dye loading and then were washed with excessive fresh medium. After incubation with a standard medium for 20 min, we observed that the filamentous Rhod-2 signals mainly colocalized with mito-GFP in melan-a melanocytes, as analyzed by IFM (Fig. 3A). At 40 min, a proportion of the Rhod-2 signals became punctate and did not colabel with mito-GFP (Fig. 3B). At 60 min, Rhod-2 signals were almost completely punctate and separated from mito-GFP-positive mitochondria (Fig. 3C). Thus, the colocalization between mito-GFP and Rhod-2 fluorescence dramatically decreased during the observation period (Fig. 3G). Furthermore, time course images also showed that the mitochondria-localized Rhod-2 signals gradually faded, and the dot-like Rhod-2 signals separated from mito-GFP-labeled mitochondria at the same time (Fig. 3I). These results suggest that Ca^{2+} -bound Rhod-2 is gradually released from mitochondria.

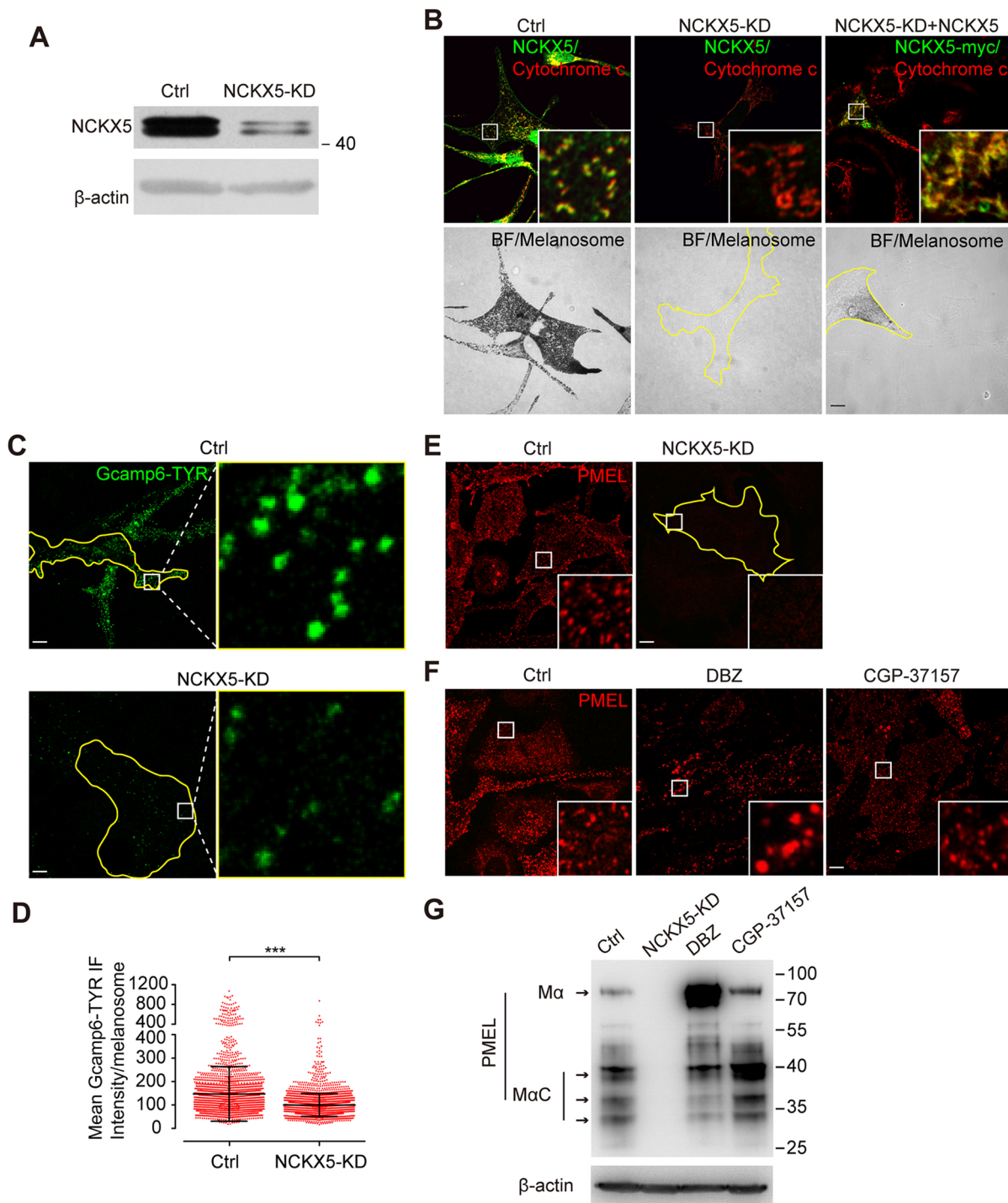


Fig. 2. Loss of NCKX5 compromises melanosomal Ca^{2+} concentration, melanosomal protein PMEL expression and melanin production.

(A) Western blot analysis of lysates from melan-a melanocytes stably expressing control shRNA (Ctrl) and melan-a melanocytes stably expressing *Nckx5* shRNA (NCKX5-KD), using NCKX5 polyclonal anti-sera. β -actin antibody was used as a loading control. (B) Confocal immunofluorescence images of Ctrl melanocytes, NCKX5-KD melanocytes and NCKX5-KD melanocytes transfected with shRNA-resistant NCKX5-Myc by colabeling with NCKX5 polyclonal anti-sera and cytochrome *c* antibody. BF images of pigmented melanosomes are also presented. Outlines of cells are indicated by yellow lines. Insets show 6 \times magnified images of the boxed region. (C) Confocal immunofluorescence images of melan-a wild-type melanocytes (WT) and NCKX5-KD melanocytes transfected with GCaMP6-TYR. Outlines of cells are indicated by yellow lines. Insets show 12 \times magnified images of the boxed region. (D) Quantification of mean fluorescent intensity of GCaMP6-TYR in WT and NCKX5-KD group; $n=2336$, and 2723 melanosomes, respectively. Each point represents the mean fluorescent intensity of a GCaMP6-TYR-labeled single melanosome. *** $P<0.001$ (Student's *t*-test). (E) Confocal immunofluorescence images of melanocytes labeled for melanosomal protein PMEL in Ctrl and NCKX5-KD melanocytes. Insets show 5 \times magnified images of the boxed region. (F) Confocal immunofluorescence images of melanocytes incubated with the compounds DMSO (Ctrl), DBZ (30 μM) or CGP-37157 (10 μM) stained for the melanosomal protein PMEL. Outlines of cells are indicated by yellow lines. Insets show 5 \times magnified images of the boxed region. (G) Western blot analysis of lysates of Ctrl melanocytes, NCKX5-KD melanocytes, and melan-a melanocytes incubated with DBZ (30 μM) or CGP-37157 (10 μM) using PMEL antibody. β -actin antibody was used as a loading control. Scale bars: 10 μm .

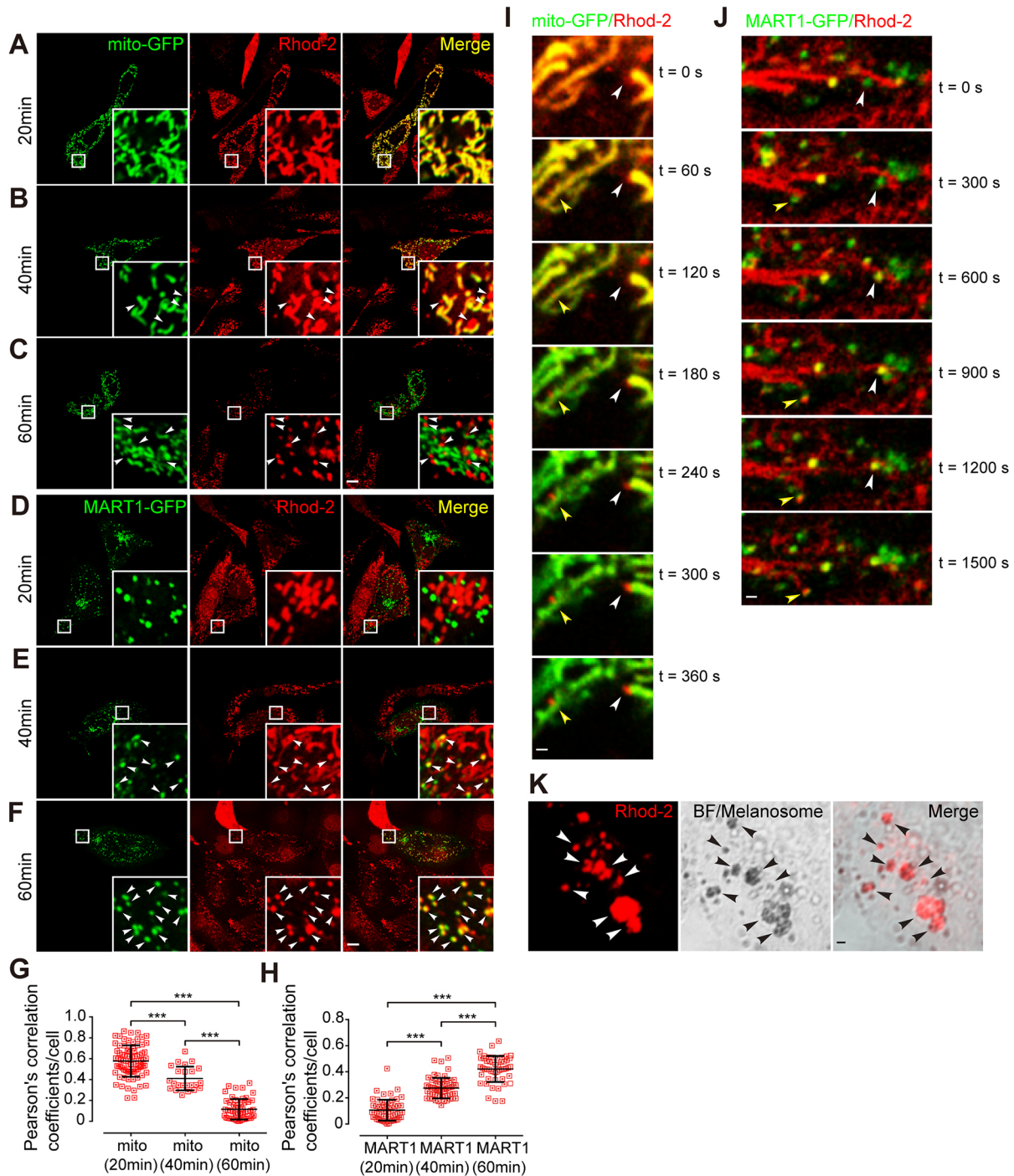


Fig. 3. Rhod-2 signals efflux from mitochondria and influx into melanosomes. (A–C) Colocalization of mito-GFP with signals from the Ca^{2+} indicator Rhod-2 at indicated time points after washing with medium (20 min, A; 40 min, B; 60 min, C) following dye loading for 30 min as analyzed by live-cell imaging in melan-a cells. Arrowheads, Rhod-2 fluorescent dots separated from mito-GFP. Insets show 6 \times magnified images of the boxed region. Scale bar: 10 μm . (D–F) Colocalization of MART1-GFP with signals from the Ca^{2+} indicator Rhod-2 at indicated time points after washing with medium (20 min, D; 40 min, E; 60 min, F) following dye loading for 30 min in melan-a cells. Arrowheads, Rhod-2 fluorescent dots colocalized with MART1-GFP. Insets show 6 \times magnified images of the boxed region. Scale bar: 10 μm . (G) Colocalization analysis (Pearson's correlation coefficient) of results shown in A–C; $n=79$, 23, and 54 cells, respectively. $***P<0.001$ (one-way ANOVA). (H) Colocalization analysis (Pearson's correlation coefficient) of results shown in D–F; $n=57$, 58, and 50 cells, respectively. $***P<0.001$ (one-way ANOVA). (I) Time course of Rhod-2 separation from mito-GFP. Arrowheads, Rhod-2 fluorescent dots separated from mito-GFP. Scale bar: 1 μm . (J) Time course of Rhod-2 colocalization with MART1-GFP. Arrowheads, Rhod-2 fluorescent dots colocalized with MART1-GFP. Scale bar: 1 μm . (K) Rhod-2 fluorescent dots colocalized with melanosomal granules. Melan-a melanocytes were labeled with Rhod-2 and visualized by BF microscopy for pigmented melanosomes. Arrowheads, Rhod-2 fluorescent dots colocalized with melanosomes. Scale bar: 1 μm .

We next transfected the melanocytes with MART1-GFP (MART1 is also known as MLANA), a protein enriched in immature melanosomes (Hoashi et al., 2005), to trace the flux of

Rhod-2 fluorescence. The colocalization of MART1-GFP and Rhod-2 fluorescence was apparently increased during the observation period (Fig. 3D–F,H). Furthermore, time course

images also showed that the dot-like Rhod-2 signals gradually colocalized with MART1-GFP-labeled melanosomes (Fig. 3J), suggesting that Rhod-2 entered into melanosomes in a time-dependent manner. In addition, the Rhod-2-positive dots visualized by bright-field (BF) microscopy overlapped well with pigment granules (Fig. 3K), confirming that the punctate dots are melanosomes.

If the Rhod-2 signal is transferred from mitochondria to melanosomes, disruption of Rhod-2/AM loading into mitochondria would compromise subsequent Rhod-2 fluorescence accumulation in melanosomes. The localization of Rhod-2/AM within mitochondria is dependent on the mitochondrial membrane potential (Babcock et al., 1997). We treated the cells with carbonyl cyanide *m*-chlorophenyl hydrazone (CCCP) to dissipate mitochondrial transmembrane potential (Ding et al., 2010). Indeed, compared to control cells, CCCP-treated cells completely lost the mitochondrial-specific Rhod-2 signals as well as the

melanosomal punctate Rhod-2 signals (Fig. 4A,B,D,E,G,H,M). After washout of CCCP, the mitochondrial Rhod-2 signals restored to some extent (Fig. 4C). Subsequently, the melanosomal Rhod-2 signals largely re-appeared (Fig. 4F,I,M). In addition, we tested whether disruption of the normal mitochondrial physiological functions would impede Rhod-2 dynamics. We inhibited mitochondrial oxidative phosphorylation by treating melanocytes with oligomycin and rotenone, respectively. In oligomycin-treated cells, the majority of Rhod-2 signals constantly colocalized with mito-GFP, and much fewer punctate Rhod-2 dots were separated from mito-GFP (Fig. 4J,K,M), suggesting that Rhod-2 is retained in mitochondria, and is not transferred to melanosomes. In oligomycin washout cells, the Rhod-2 signals were punctate and were clearly separated from mito-GFP, resembling the control group (Fig. 4L, M). Rotenone has similar inhibitory effects in melanocytes (Fig. 4M). Taken together, these results suggest that Rhod-2 is transferred from mitochondria into melanosomes in melan-

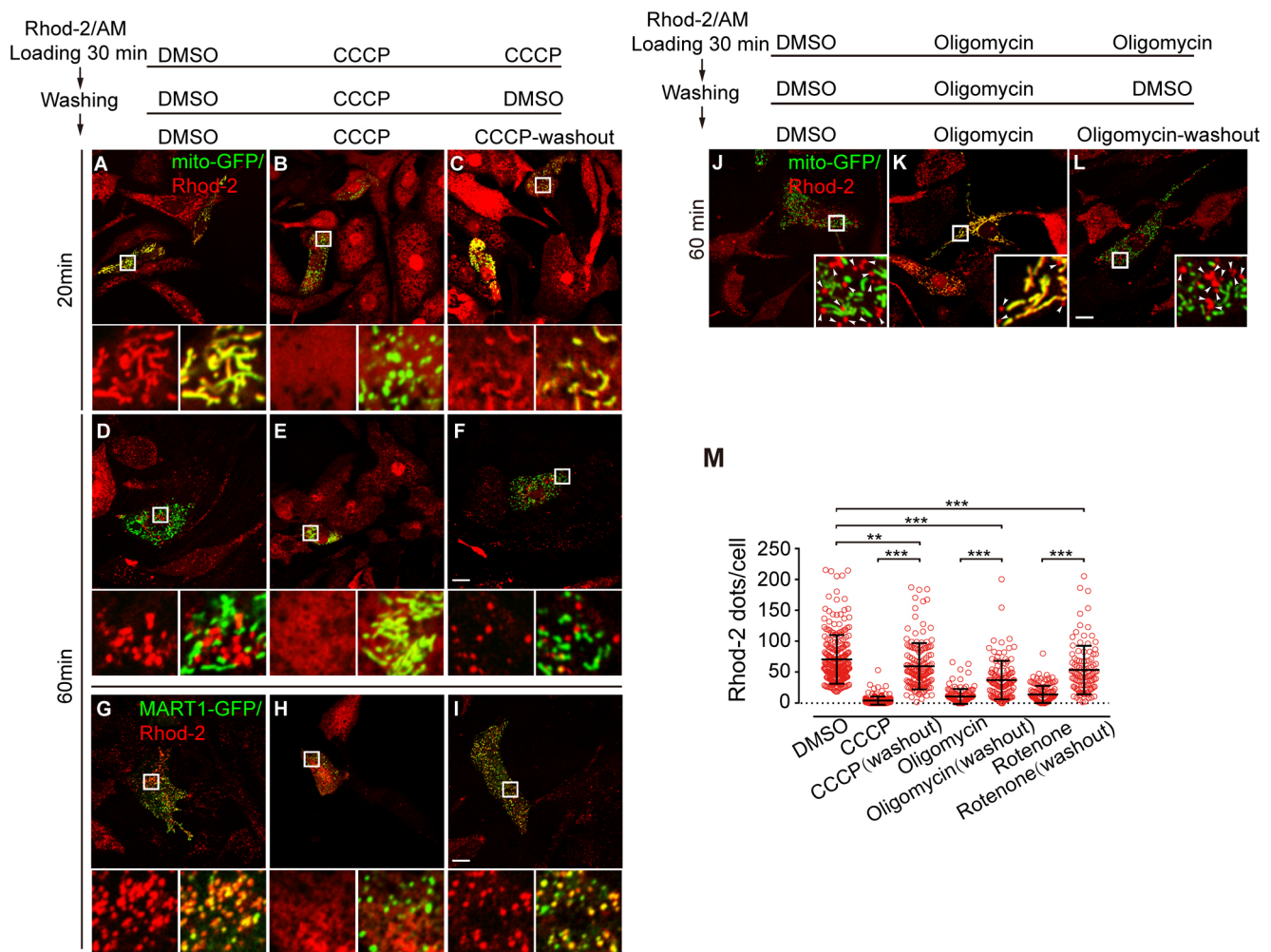


Fig. 4. Functional mitochondria are required for mitochondrial Rhod-2 transfer to melanosomes. (A–F) Confocal immunofluorescence images of melan-a melanocytes transfected with mito-GFP and labeled with Rhod-2 in the presence of DMSO (control) or 10 μ M CCCP, as indicated. All the time points are time after washing with the indicated medium following dye loading for 30 min. Insets show 6 \times magnified images of the boxed region. Scale bar: 10 μ m. (G–I) Confocal immunofluorescence images of melan-a melanocytes transfected with MART1-GFP and labeled with Rhod-2 in the presence of DMSO (control) or 10 μ M CCCP, respectively, 60 min after dye loading (for 30 min) and washing with indicated medium. Insets show 6 \times magnified images of the boxed region. Scale bar: 10 μ m. (J–L) Confocal immunofluorescence images of melanocytes transfected with mito-GFP then labeled with Rhod-2 in the presence of indicated compounds (60 min after washing with indicated medium following dye loading for 30 min): DMSO (J); oligomycin 10 μ M (K); oligomycin 10 μ M washout (L). Arrowheads, Rhod-2 dots separated from mito-GFP. Insets show 6 \times magnified images of the boxed region. Scale bar: 10 μ m. (M) Quantification of the number of Rhod-2 dots in a single cell (60 min after wash) for each treatment; $n=245, 170, 149, 123, 117, 130,$ and 107 cells, respectively. ** $P<0.01$; *** $P<0.001$ (one-way ANOVA).

melanocytes in a manner that is dependent on functional mitochondria.

Similar to what we found with Rhod-2, we found that another Ca^{2+} tracer, X-Rhod-1, could be transferred from mitochondria to melanosomes (Fig. 5A,C,E,G,I,J). In contrast, the mitochondrial dye mitotracker CMXRos and an analog of Rhod-2/AM, Rhodamine 123, which possess similar fluorophores to X-Rhod-1 or Rhod-2 but lack the Ca^{2+} -binding radical, were constantly trapped in mitochondria (Fig. 5B,D,F,H). These results suggest that the Ca^{2+} -binding fluorophores are required for the specific transfer of X-Rhod-1 or Rhod-2 from mitochondria to melanosomes. This establishes a unique tool for monitoring the transfer of mitochondrial Ca^{2+} signal into melanosomes or other Ca^{2+} -enriched organelles (data not shown). Our results suggest that ions such as Ca^{2+} are transferred into melanosomes from mitochondria, which provides another source of Ca^{2+} .

Disruption of NCKX5 and NCKX activity compromise Rhod-2 loading in melanosomes and pigment production

To test whether loss of NCKX5 affects Ca^{2+} flow from mitochondria to melanosomes in melanocytes, NCKX5-KD cells were transfected with mito-GFP or MART1-GFP to trace the subcellular localization of Rhod-2 fluorescence. In control cells, the Rhod-2 fluorescence overlapped with mito-GFP at the beginning of the observation period and then with MART1-GFP later (Fig. 6A,E). In contrast, in NCKX5-KD cells, Rhod-2 fluorescence overlapped with mito-GFP at the start, while fewer Rhod-2 puncta overlapped with MART1-GFP during the observation period during which the intensity decreased (Fig. 6B,F,I), suggesting that Ca^{2+} signal flow from mitochondria to melanosomes is impeded. These results are consistent with the reduced melanosomal Ca^{2+} concentration, as determined by analyzing GCaMP6-TYR in NCKX5-KD cells (Fig. 2C,D).

Consistent with our findings of impaired PMEL processing in NCKX5-KD cells (shown in Fig. 2E,G), the NCKX inhibitor DBZ did not disrupt Rhod-2 release from mitochondria, but attenuated Rhod-2 accumulation in melanosomes (Fig. 6C,G,J), suggesting

that the NCKX activity is required for Ca^{2+} transfer from mitochondria to melanosomes. By contrast, the Rhod-2 signals were retained in mitochondria treated with the NCLX inhibitor CGP-37157, but did not attenuate Rhod-2 accumulation in melanosomes (Fig. 6D,H,K), consistent with the finding that blocking NCLX activity likely inhibits mitochondrial Ca^{2+} extrusion into cytosol (Palty et al., 2010). Furthermore, NCKX activity depends on the K^+ gradient for exchange of Ca^{2+} (Schnetkamp, 2013). We speculated that depletion of K^+ in the medium may attenuate the efflux of Rhod-2 signals. Indeed, K^+ deprivation did not influence the Rhod-2 signal separation from mito-GFP-labeled mitochondria but, apparently, attenuated Rhod-2 accumulation in melanosomes. The number of Rhod-2-loaded melanosomes was dramatically reduced along with sequential declining K^+ levels (Fig. 7), suggesting that K^+ deprivation does not block the Ca^{2+} efflux from mitochondria, but may attenuate Ca^{2+} signal accumulation in melanosomes. Taken together, our results suggest that NCKX5 and NCKX activity are required for Ca^{2+} signal flow from mitochondria to melanosomes.

Consistent with the inhibitory effects on mitochondrial Ca^{2+} transfer to melanosomes, we observed a dramatic inhibition of melanin synthesis in the DBZ-treated but not in the CGP-37157-treated melanocytes (Fig. 8A–D,I), suggesting that NCKX but not NCX activity is required for melanogenesis. In addition, CCCP-, oligomycin- or rotenone-treated cells exhibited an apparent reduction of melanin content. In contrast, the lysosomal protease inhibitor leupeptin (Niel et al., 2011) had no obvious inhibitory effect on melanin synthesis (Fig. 8E–H,J). These results suggest that functional mitochondria and the NCKX activity are required for melanogenesis, which establishes the functional link between mitochondria and melanosomes.

Taken together, our data suggest that there are substance exchanges between mitochondria and melanosomes, and loss of mitochondrial NCKX5 likely attenuates Ca^{2+} enrichment in melanosomes, which compromises melanosome maturation and pigment production.

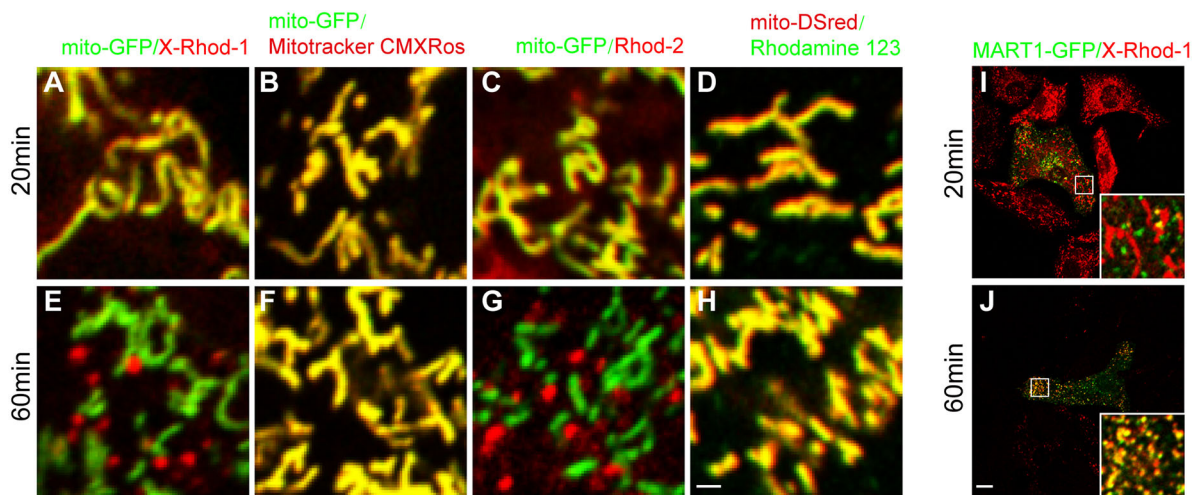


Fig. 5. X-Rhod-1 and Rhod-2 specifically efflux from mitochondria and influx into melanosomes. (A–D) Images of melanocytes transfected with mito-GFP and labeled with chemical compound dyes (20 min after washing with medium following dye loading for 30 min): X-Rhod-1 (A); mitotracker CMXRos (B); Rhod-2 (C) and Rhodamine 123 (D). (E–H) Images of melanocytes transfected with mito-GFP and labeled with indicated chemical compound dyes (60 min after washing with medium following dye loading for 30 min): X-Rhod-1 (E); mitotracker CMXRos (F); Rhod-2 (G) and Rhodamine 123 (H). Scale bar: 1 μm . (I) Images of melanocytes transfected with MART1-GFP and labeled with X-Rhod-1 at 20 min after washing with medium following dye loading for 30 min. (J) Images of melanocytes transfected with MART1-GFP and labeled with X-Rhod-1 at 60 min after washing with medium following dye loading for 30 min. Scale bar: 10 μm .

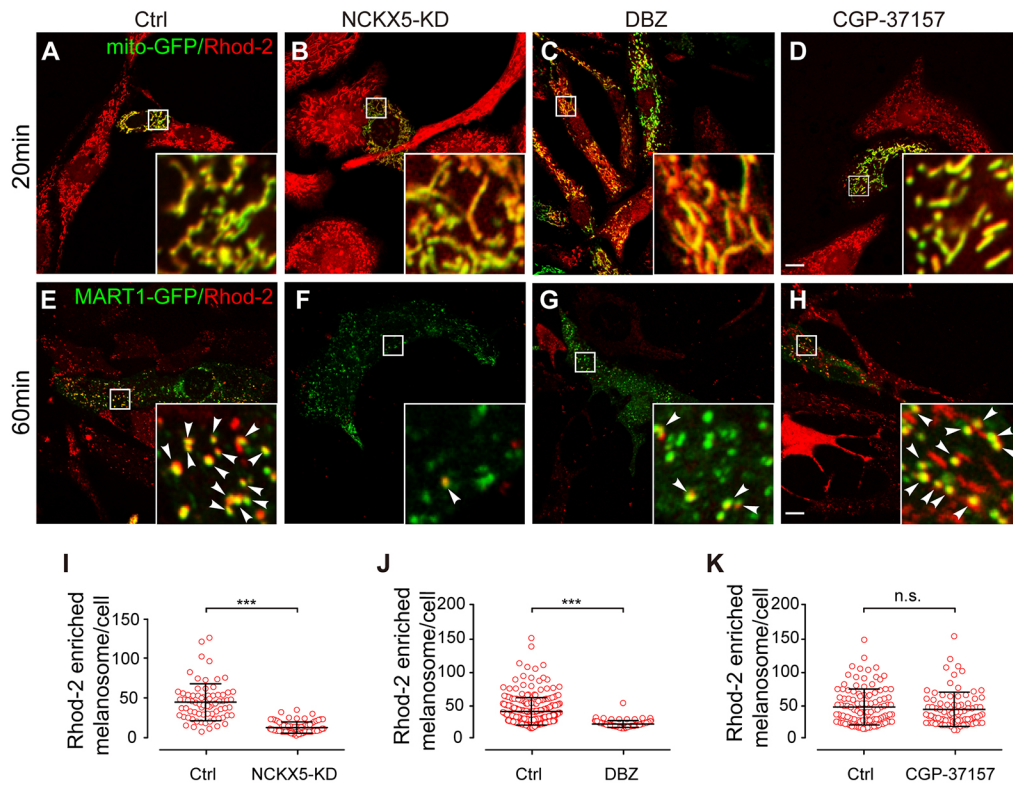


Fig. 6. NCKX5 and NCKX activity are required for Rhod-2 signal accumulation in melanosomes. (A–D) Images of melanocytes transfected with mito-GFP and labeled with Rhod-2 (20 min after washing with medium following dye loading for 30 min): control (A), NCKX5-KD (B), or after treatment with DBZ (30 μ M) (C), or CGP-37157 (10 μ M) (D). Insets show 6 \times magnified images of the boxed region. Scale bar: 10 μ m. (E–H) Images of melanocytes transfected with MART1-GFP and labeled with Rhod-2 (60 min after washing with medium following dye loading for 30 min): control (E), NCKX5-KD (F), or after treatment with DBZ (30 μ M) (G) or CGP-37157 (10 μ M) (H). Insets show 6 \times magnified images of the boxed region. Scale bar: 10 μ m. (I) Quantification of the number of Rhod-2 fluorescent dots colocalized with MART1-GFP (60 min after washing) in control and NCKX5-KD group; $n=74$, and 78 cells, respectively. Each point represents the number of Rhod-2 and MART1-GFP colabeled dots in a single cell. $***P<0.001$ (Student's t -test). (J) Quantification of the number of Rhod-2 fluorescent dots colocalized with MART1-GFP (60 min after washing) in the control and DBZ treatment (30 μ M) group; $n=268$, and 94 cells, respectively. Each point represents the number of Rhod-2 and MART1-GFP colabeled dots in a single cell. $***P<0.001$ (Student's t -test). (K) Quantification of the number of Rhod-2 fluorescent dots colocalized with MART1-GFP (60 min after washing) in the control and CGP-37157 treatment (10 μ M) group; $n=114$, and 86 cells, respectively. Each point represents the number of Rhod-2 and MART1-GFP colabeled dots in a single cell. n.s., not significant (Student's t -test).

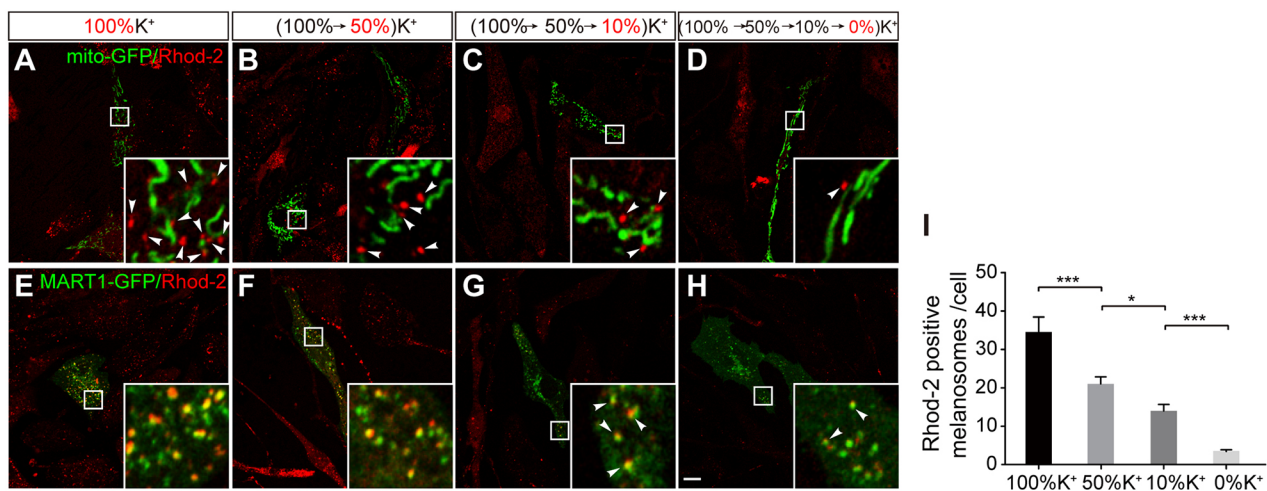


Fig. 7. NCKX activity is required for Rhod-2 loading in melanosomes. (A–D) Images of melanocytes transfected with mito-GFP and rinsed with 100% K⁺-containing or with a series of K⁺-depleted buffers, then labeled with Rhod-2 (60 min after wash); the final K⁺ concentration in each treatment is presented in red: 100% K⁺ (control, A); 50% K⁺ (B); 10% K⁺ (C); 0% K⁺ (D). (E–H) Images of melanocytes transfected with MART1-GFP and rinsed with 100% K⁺-containing or with a series of K⁺-depleted buffers, then labeled with Rhod-2 (60 min after wash); the final K⁺ concentration in each treatment is presented in red: 100% K⁺ (control, E); 50% K⁺ (F); 10% K⁺ (G); 0% K⁺ (H). Scale bar: 10 μ m. Arrowheads represent colocalization with Rhod-2. (I) Quantification of the number of Rhod-2 fluorescent dots colocalized with MART1-GFP in a single melanocyte for experiments as in E–H; $n=96$, 111, 163, and 147 cells, respectively. $*P<0.05$; $***P<0.001$ (Student's t -test).

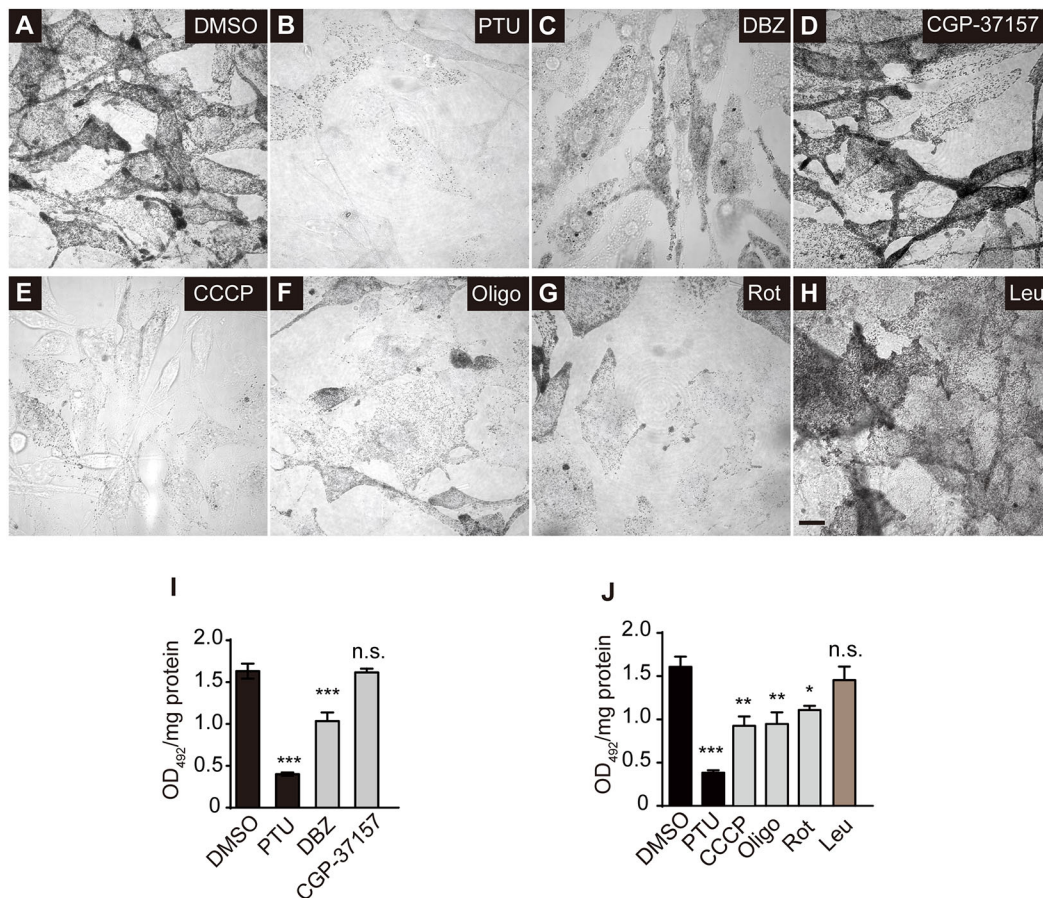


Fig. 8. NCKX activity and functional mitochondria are required for melanosomal pigment production. (A–H) Confocal BF images of melan-a melanocytes incubated with corresponding compounds for 72 hours: DMSO (A); phenylthiourea (PTU, 200 nM) (B); DBZ (30 μ M) (C); CGP-37157 (10 μ M) (D); CCCP (2 μ M) (E); Oligomycin (Oligo, 5 μ M) (F); Rotenone (Rot, 0.4 μ M) (G); and Leupeptin (Leu, 100 mM) (H). Scale bar: 10 μ m. (I) Melanin quantification assays for melanocytes incubated with PTU (200 nM), DBZ (30 μ M) and CGP-37157 (10 μ M). Melanin content was assayed by measuring optical density at 492 nm (OD₄₉₂). Assays were performed in triplicate. (J) Melanin quantification assays for melanocytes incubated with PTU (200 nM); CCCP (2 μ M); Oligo (5 μ M); Rot (0.4 μ M); Leu (100 mM). Melanin content was assayed by measuring optical density at 492 nm (OD₄₉₂). Assays in I and J were performed in triplicate. Data shown are means \pm s.e.m. of the number of triplicate experiments. n.s., not significant; * P <0.05; ** P <0.01; *** P <0.001 (Student's *t*-test).

DISCUSSION

Previous studies demonstrated that NCKX5 may be localized to TGN or melanosomes; here, we have shown that NCKX5 is localized to mitochondria and TGN (but not melanosomes) in melanocytes. Several studies have reported the subcellular localization of NCKX5 in pigment cells, but conflicting data have been presented. In human melanoma MNT1 cells, GFP-tagged and HA-tagged zebrafish NCKX5 exhibited an intracellular localization (Lamason et al., 2005). There was no organellar marker colabeled in the MNT1 cells, but the distributional pattern did not look like a TGN pattern. Proteomic analysis in MNT1 cells reveals that NCKX5 is present in melanosomes (Chi et al., 2006). However, those authors also estimated that melanosome fractions are contaminated with 1–6% mitochondrial proteins. Similarly, we also found that the mitochondrial fraction in melanocytes was always black, which is indicative of mixture of melanosomes (data not shown). This suggests that mitochondria and melanosomes may have overlapping sediment features and co-exist largely in the same fraction, which may explain the identification of NCKX5 in melanosomes by proteomic analysis (Chi et al., 2006). Unfortunately, Chi et al. did not prove its melanosomal localization by IFM. In normal human epidermal melanocytes (NHMs), endogenous human NCKX5, which was detected by

polyclonal antisera, was reported to be partially localized to TGN (Ginger et al., 2008). Those authors did not mention the additional signals outside of TGN. Our investigation indicated the additional signals were localized to mitochondria. Recently, overexpressed NCKX5 has been reported to be exclusively located in the TGN in MNT1 cells (Rogasevskaia et al., 2019). We have shown an exclusive TGN localization of overexpressed NCKX5 in ~30% melanocytes (Fig. 1L–N). Therefore, we conclude that NCKX5 localizes to both the TGN and mitochondria, but not to melanosomes. Considering that TGN-localized NCKX5 is transported by the secretory pathway, whereas the mitochondrial NCKX5 is not, we speculate that there may be two isoforms of NCKX5, with or without the predicted N-terminal 29-residue signal peptide that would modulate targeting. However, this awaits further investigation.

In this study, we have demonstrated that mitochondrial NCKX5 plays a pivotal role in regulating melanogenesis, although we have not excluded a possible contribution of the TGN-localized NCKX5 to melanogenesis. The pathogenesis of OCA has been classified into two categories. One lacks melanosomal protein; the other is deficient in melanosomal protein trafficking complexes (Wei and Li, 2013). We have excluded the melanosomal localization of NCKX5. The transmembrane features of NCKX5 argue that it

behaves like a trafficking protein for melanosomal proteins. Thus, we have defined a new class of OCA caused by dysfunctional mitochondria, which we refer to as 'mitochondrial OCA'. With this regard, it is predicted that deficiency in other mitochondrial components coupling to NCKX5 or with an effect on mitochondrial homeostasis could likewise produce a hypopigmentation phenotype. We confirmed that NCKX5 is partially localized to TGN, but the physiological functions of TGN-targeted NCKX5 need further investigation.

There are several hypotheses on the graying of hair with aging, ranging from melanocyte and melanogenic stem cell death to reduction in melanin synthesis. Reactive oxygen species (ROS)-induced damage has been suggested. However, the precise mechanism(s) remain unknown (Seiberg, 2013). Mitochondria are both a major source and a primary target of toxic ROS within cells, especially when excessive ROS is produced during melanogenesis, thus playing a pivotal role in aging and stress sensing (Harman, 1972). Similarly, in some vitiligo patients, melanocytes and melanosomes exist but pigment production is inhibited (Ezzedine et al., 2015). Mitochondrial function is impaired in vitiligo melanocytes (Dell'Anna et al., 2001; Laddha et al., 2013). Inhibition of mitochondrial function may explain the hypopigmentation in these aged and/or stressed melanocytes.

Mitochondrion–melanosome contact sites may have functions in exchanging Ca^{2+} and other molecules such as ATP, lipids or proteins required for melanosome biogenesis or melanin biosynthesis. NCKX5 may act as a key protein mediating mitochondrial Ca^{2+} efflux, and be important for Ca^{2+} homeostasis within both mitochondria and melanosomes. It is unknown whether NCKX5 localizes at the mitochondrion–melanosome contact sites or whether it is coupled with another Ca^{2+} influx protein on melanosomes, to directly mediate Ca^{2+} transport. This machinery awaits further investigation. Our findings expand our knowledge of the functions of the mitochondrial interactome, indicating that the mitochondrion is another organellar Ca^{2+} source, as well as, for example, the ER, through which Ca^{2+} can be transferred through organelle interactions.

MATERIALS AND METHODS

DNA constructs

The full-length cDNA of mouse *Nckx5* was amplified from melan-a total RNA. To construct pNCKX5, the entire *Nckx5* cDNA was subcloned into the *EcoRI* and *XhoI* sites of pcDNA3.1(+) (Invitrogen). To generate epitope-tagged pNCKX5, the Myc epitope tag was inserted between Ser52 and Glu53 of the NCKX5 to generate pNCKX5-myc based on a scheme in a previous study (Ginger et al., 2008). The full-length cDNA of mouse *Mart1* was amplified from melan-a total RNA. To construct MART1–GFP, the entire *Mart1* cDNA was subcloned into the *XhoI* and *EcoRI* sites of pEGFP-N2 (Clontech). The cDNA of mouse *Cox8a* was amplified from mouse liver total RNA. To construct mito-GFP, the signal peptide of *Cox8a*, corresponding to amino acids 1–25, was subcloned into the *XhoI* and *EcoRI* sites of pEGFP-N2 (Clontech). The full-length cDNA of mouse tyrosinase was amplified from melan-a total RNA. To construct GCaMP6–TYR, the entire tyrosinase cDNA was subcloned into the *HindIII* and *XbaI* sites of pGP-CMV-GCaMP6m (Addgene).

Generation of NCKX5-KD melan-a melanocytes

shRNAs against mouse *Nckx5* gene (NCBI RefSeq NM_175034.3) were designed with the siRNA target finder (Ambion, Austin, TX). Oligodeoxyribonucleotide duplexes containing the target sequences were synthesized and introduced into the *BamHI* and *HindIII* sites of the expression plasmid pSilencer 5.1-H1 Retro vector (Ambion). The target sequences were as follows: shNCKX5, 5'-GCTGGAACTAGACCGAA-A-3', and for scramble control, 5'-AATTCTCCGAACGTGTCACGT-3'.

To generate shRNA-resistant NCKX5, five silent mutations were introduced into pNCKX5-myc by site-directed mutagenesis, changing the sites from 5'-GGCTGGAACTAGACCGAAAG-3' to 5'-GGCTGGAAAGTTGGATA-GAAAG-3' (silent mutations are underlined). Melan-a melanocytes were seeded in a 35×10 mm dish at 2.0×10⁵ cells 24 h prior to transfection. The vectors were transfected into cells using Fugene 6 (Promega) following the manufacturer's instructions. After 24 h, the transfected cell clone expressing the vector was selected by treatment with 2.5 mg/ml of puromycin (InvivoGen).

Cell culture and transfections

Immortalized melan-a melanocytes (Bennett et al., 1987) were obtained from the Wellcome Trust Functional Genomics Cell Bank. Melan-a cells were grown at 37°C and 10% CO₂ in RPMI 1640 (Hyclone) with 10% fetal bovine serum (FBS) (Hyclone), 1% penicillin-streptomycin (P/S) and 200 nM phorbol 12-myristate-13-acetate (Sigma-Aldrich). NCKX5-KD melanocytes were maintained in RPMI 1640 with 10% FBS, 1% P/S, 200 nM phorbol 12-myristate-13-acetate and 2 mg/ml puromycin (InvivoGen). Melan-a melanocytes were transfected by using Fugene 6 (Promega) according to the manufacturer's instructions with 1–2 µg of DNA. NCKX5-KD cells were transfected by using the Neon transfection system (Life Technologies) according to manufacturer's instructions with 1–2 µg of DNA.

Antibodies

NCKX5(A1) polyclonal anti-sera were generated in rabbits against synthetic peptides corresponding to amino acids 253–268 of the mouse NCKX5. NCKX5(B1) polyclonal anti-sera were generated in rabbits against synthetic peptides corresponding to amino acids 492–501 of the mouse NCKX5. NCKX5(C4) polyclonal anti-sera against mouse NCKX5 was generated by immunizing rabbits with a purified His-tagged fusion protein corresponding to amino acids 210–306 of the mouse NCKX5. The following antibodies were used in this study: mouse anti-TYRP1 (Covance, MEL5, 1:500), mouse anti-cytochrome *c* (BD, 556432, 1:1,000), mouse anti-PMEL (Thermo, HMB45, 1:200), mouse anti-Myc (Huaxingbio, HX1802, 1:1000), rabbit anti-Myc (MBL, 562, 1:500), rat anti-LAMP1 (BD, 553792, 1:500), rabbit anti-TGN38 (Santa Cruz Biotechnology, sc-33784, 1:200), mouse anti-β-actin (Sigma-Aldrich, A5441, 1:20,000).

Immunoblotting

Immortalized melanocytes were washed with ice-cold PBS, re-suspended in lysis buffer (50 mM Tris-HCl pH 7.4, 150 mM NaCl and 1% Triton X-100) in the presence of a protease inhibitor cocktail (Sigma-Aldrich). After 60 min incubation on ice, cell lysates were centrifuged at 13,000 g for 15 min at 4°C to remove cell debris. Equal amounts of homogenates were separated on 10% SDS-PAGE gels and transferred onto polyvinylidene difluoride (PVDF, Millipore) membranes. The membrane was then blocked with blocking buffer (5% skimmed milk and 0.1% Tween 20 in PBS) and incubated with primary antibody overnight at 4°C. Blots were incubated with the appropriate horseradish peroxidase (HRP)-conjugated secondary antibodies for 1.5 h at room temperature and visualized by ECL (Pierce, Rockford, IL).

Immunofluorescence microscopy

Mouse melanocytes were seeded at 0.5×10⁵ per well in 12-well dishes on coverslips. After an overnight incubation, cells were transfected with expression plasmids for 24–48 h. After washing twice with PBS, cells were fixed with 4% (w/v) paraformaldehyde for 10 min at room temperature or fixed with pre-chilled acetone for 5 min at 4°C, and then permeabilized for 10 min with 0.2% Triton X-100 in PBS. Blocking was performed with 1% BSA in PBS for 1 h, then incubated with indicated primary antibodies in PBS containing 1% BSA for 12 h at 4°C. After extensive rinses, cells were subsequently washed and incubated for 1 h with secondary antibody at room temperature. Confocal images were acquired using a 100× oil objective with NA 1.40 on a Nikon confocal microscope (ECLIPSE Ti-C2, Japan). Images were obtained using the NIS-Elements AR 3.2 software provided by Nikon.

Inhibitor treatment

For inhibitor treatment, cells were loaded for 30 min with 2.5 μM Rhod-2/AM, concomitant with treatment compounds, including 10 μM CCCP (Sigma-Aldrich), 10 μM oligomycin (Selleck), 2 μM rotenone (Sigma-Aldrich), 10 μM , 20 μM , and 30 μM 3',4'-dichlorobenzamil hydrochloride (DBZ; Sigma-Aldrich). Cells were then rinsed with medium containing DMSO or indicated compounds. The subsequent mitochondrial and melanosomal Ca^{2+} measurements were undertaken as described below.

Fluorescent Ca^{2+} imaging

Mouse melanocytes were seeded at 0.5×10^4 per well in Nunc™ Lab-Tek™ chambered cover glass (Thermo). For the GFP-based Ca^{2+} indicator, the melanocytes were transfected with GCaMP6–TYR for 24 h, then the fluorescence intensity was determined through confocal microscopy. For chemical-compound Ca^{2+} dyes, cells were loaded for 30 min with 2.5 μM Rhod-2/AM or X-Rhod-1/AM (Invitrogen), respectively. Following dye loading, cells were then rinsed with full-serum RPMI-1640 medium. For mitochondrial Ca^{2+} measurement, the cells were further incubated at 37°C for 20 min, then mounted in the cell chamber of the confocal microscope. For measurements of melanosomal Ca^{2+} , the cells were incubated at 37°C for 40 or 60 min, then mounted in the cell chamber.

K^+ depletion

K^+ depletion experiments were performed as described previously with modifications (Kiyoshima et al., 2011; Puri et al., 2001). In the control group, melan-a melanocytes were maintained in 100% K^+ -containing buffer [103.4 mM NaCl, 5.3 mM KCl, 23.8 mM NaHCO_3 , 5.6 mM Na_2HPO_4 , 0.4 mM MgSO_4 , 0.423 mM $\text{Ca}(\text{NO}_3)_2$, 11.1 mM D-glucose, pH 7.4, 2% BSA] and incubated with Rhod-2/AM. In 50%, 10% and 0% K^+ -containing buffers, KCl was replaced by NaCl. In K^+ -reduced or -free groups, K^+ was gradually decreased to the indicated concentrations by following the order of 100%, 50%, 10%, and 0%. Taking the 0% K^+ group, for example, melan-a melanocytes were incubated sequentially with 100%, 50%, 10%, K^+ -containing buffers at 2 min intervals and then incubated with Rhod-2/AM in 0% K^+ -containing buffer.

Melanin measurement

Melanocytes were pretreated with the tyrosinase inhibitor phenylthiourea (PTU) (200 nM) for 3 days for depigmentation. Cells were further treated with PTU (positive control) and DMSO (negative control) or cultured in the presence of indicated compounds [2 μM CCCP (Sigma-Aldrich), 5 μM oligomycin (Selleck), 0.4 μM rotenone (Sigma-Aldrich), 30 μM 3',4'-dichlorobenzamil hydrochloride (DBZ; Sigma-Aldrich), 10 μM CGP-37157 (Tocris) or 100 mM leupeptin (Sigma-Aldrich)] for 3 days. Melanin quantification was performed as previously described (Wasmeier et al., 2006). Briefly, the cells were harvested and washed in PBS, then pelleted and solubilized in 50 mM Tris-HCl pH 7.4, 2 mM EDTA, 150 mM NaCl, 1 mM dithiothreitol and protease inhibitors. The protein content of the supernatant was determined as optical density at 595 nm. Pigment was pelleted by centrifugation at 16,000 g for 10 min at 4°C, then rinsed once in ethanol:ether (1:1), and dissolved in 2 M NaOH with 20% DMSO at 60°C. Melanin content was measured as the optical density at 492 nm, and normalized to their protein content.

Statistical analysis

All data are shown as mean \pm s.e.m. in column bar graphs, and as mean \pm s.d. in scatter plots. Statistical analyses were performed with Student's *t*-test or one-way ANOVA with a post-Tukey's multiple comparison test. Differences were considered statistically significant when $P < 0.05$. Pearson's coefficients were calculated with the NIS-Elements AR 3.2 software (Nikon).

Acknowledgements

We thank Drs Richard Swank and Quan Chen for their comments and for proofreading this manuscript.

Competing interests

The authors declare no competing or financial interests.

Author contributions

Conceptualization: W.L.; Methodology: E.S.; Investigation: Z.Z., J.G.; Resources: E.S., A.W.; Writing - original draft: Z.Z., W.L.; Writing - review & editing: W.L.; Supervision: A.W., W.L.; Project administration: Z.Z., A.W., W.L.; Funding acquisition: A.W., E.V.S., W.L.

Funding

This work was partially supported by grants from the National Natural Science Foundation of China (#31830054 to W.L.; #81472871 to A.W.; #91539204 to W.L.), the Ministry of Science and Technology of the People's Republic of China (#2016YFC1000306) (to W.L.), and the Wellcome Trust (#108429 to E.V.S.). Deposited in PMC for release after 6 months.

References

- Altimimi, H. F., Szerencsei, R. T. and Schnetkamp, P. P. M. (2013). Functional and structural properties of the NCKX2 Na(+)-Ca (2+)/K (+) exchanger: a comparison with the NCX1 Na (+)/Ca (2+) exchanger. *Adv. Exp. Med. Biol.* **961**, 81-94. doi:10.1007/978-1-4614-4756-6_8
- Ammann, S., Schulz, A., Krageloh-Mann, I., Dieckmann, N. M. G., Niethammer, K., Fuchs, S., Eckl, K. M., Plank, R., Werner, R., Altmüller, J. et al. (2016). Mutations in AP3D1 associated with immunodeficiency and seizures define a new type of Hermansky-Pudlak syndrome. *Blood* **127**, 997-1006. doi:10.1182/blood-2015-09-671636
- Babcock, D. F., Herrington, J., Goodwin, P. C., Park, Y. B. and Hille, B. (1997). Mitochondrial participation in the intracellular Ca^{2+} network. *J. Cell Biol.* **136**, 833-844. doi:10.1083/jcb.136.4.833
- Bennett, D. C., Cooper, P. J. and Hart, I. R. (1987). A line of non-tumorigenic mouse melanocytes, syngeneic with the B16 melanoma and requiring a tumour promoter for growth. *Int. J. Cancer* **39**, 414-418. doi:10.1002/ijc.2910393024
- Berridge, M. J., Lipp, P. and Bootman, M. D. (2000). The versatility and universality of calcium signalling. *Nat. Rev. Mol. Cell Biol.* **1**, 11-21. doi:10.1038/35036035
- Berson, J. F., Harper, D. C., Tenza, D., Raposo, G. and Marks, M. S. (2001). Pmel17 initiates premelanosome morphogenesis within multivesicular bodies. *Mol. Biol. Cell* **12**, 3451-3464. doi:10.1091/mbc.12.11.3451
- Berson, J. F., Theos, A. C., Harper, D. C., Tenza, D., Raposo, G. and Marks, M. S. (2003). Proprotein convertase cleavage liberates a fibrillogenic fragment of a resident glycoprotein to initiate melanosome biogenesis. *J. Cell Biol.* **161**, 521-533. doi:10.1083/jcb.200302072
- Blaustein, M. P. and Lederer, W. J. (1999). Sodium calcium exchange: Its physiological implications. *Physiol. Rev.* **79**, 763-854. doi:10.1152/physrev.1999.79.3.763
- Burgoyne, T., Patel, S. and Eden, E. R. (2015). Calcium signaling at ER membrane contact sites. *Biochim. Biophys. Acta* **1853**, 2012-2017. doi:10.1016/j.bbamcr.2015.01.022
- Bush, W. D. and Simon, J. D. (2007). Quantification of Ca(2+) binding to melanin supports the hypothesis that melanosomes serve a functional role in regulating calcium homeostasis. *Pigment Cell Res.* **20**, 134-139. doi:10.1111/j.1600-0749.2007.00362.x
- Chi, A., Valencia, J. C., Hu, Z.-Z., Watabe, H., Yamaguchi, H., Mangini, N. J., Huang, H., Canfield, V. A., Cheng, K. C., Yang, F. et al. (2006). Proteomic and bioinformatic characterization of the biogenesis and function of melanosomes. *J. Proteome Res.* **5**, 3135-3144. doi:10.1021/pr060363j
- Cox, D. A., Conforti, L., Sperelakis, N. and Matlib, M. A. (1993). Selectivity of inhibition of $\text{Na}^+/\text{Ca}^{2+}$ exchange of heart-mitochondria by benzothiazepine cgp-37157. *J. Cardiovasc. Pharm.* **21**, 595-599. doi:10.1097/00005344-199304000-00013
- Daniele, T., Hurbain, I., Vago, R., Casari, G., Raposo, G., Tacchetti, C. and Schiaffino, M. V. (2014). Mitochondria and melanosomes establish physical contacts modulated by Mfn2 and involved in organelle biogenesis. *Curr. Biol.* **24**, 393-403. doi:10.1016/j.cub.2014.01.007
- Dell'Anna, M. L., Maresca, V., Briganti, S., Camera, E., Falchi, M. and Picardo, M. (2001). Mitochondrial impairment in peripheral blood mononuclear cells during the active phase of vitiligo. *J. Invest. Dermatol.* **117**, 908-913. doi:10.1046/j.0022-202x.2001.01459.x
- Ding, W.-X., Ni, H.-M., Li, M., Liao, Y., Chen, X., Stolz, D. B., Dorn, G. W., II and Yin, X.-M. (2010). Nix is critical to two distinct phases of mitophagy, reactive oxygen species-mediated autophagy induction and Parkin-ubiquitin-p62-mediated mitochondrial priming. *J. Biol. Chem.* **285**, 27879-27890. doi:10.1074/jbc.M110.119537
- Ezzedine, K., Eleftheriadou, V., Whitton, M. and van Geel, N. (2015). Vitiligo. *The Lancet* **386**, 74-84. doi:10.1016/S0140-6736(14)60763-7
- Fonteriz, R. I., de la Fuente, S., Moreno, A., Lobatón, C. D., Montero, M. and Alvarez, J. (2010). Monitoring mitochondrial $[\text{Ca}^{2+}]$ dynamics with rhod-2, ratiometric percam and aequorin. *Cell Calcium* **48**, 61-69. doi:10.1016/j.ceca.2010.07.001
- Garrity, A. G., Wang, W., Collier, C. M. D., Levey, S. A., Gao, Q. and Xu, H. (2016). The endoplasmic reticulum, not the pH gradient, drives calcium refilling of lysosomes. *eLife* **5**, 15887. doi:10.7554/eLife.15887

- Ginger, R. S., Askew, S. E., Ogborne, R. M., Wilson, S., Ferdinando, D., Dadd, T., Smith, A. M., Kazi, S., Szerencsei, R. T., Winkfein, R. J. et al. (2008). SLC24A5 encodes a trans-Golgi network protein with potassium-dependent sodium-calcium exchange activity that regulates human epidermal melanogenesis. *J. Biol. Chem.* **283**, 5486-5495. doi:10.1074/jbc.M707521200
- Harman, D. (1972). The biologic clock: the mitochondria? *J. Am. Geriatr. Soc.* **20**, 145-147. doi:10.1111/j.1532-5415.1972.tb00787.x
- Hoashi, T., Watabe, H., Muller, J., Yamaguchi, Y., Vieira, W. D. and Hearing, V. J. (2005). MART-1 is required for the function of the melanosomal matrix protein PMEL17/GP100 and the maturation of melanosomes. *J. Biol. Chem.* **280**, 14006-14016. doi:10.1074/jbc.M413692200
- Hoashi, T., Muller, J., Vieira, W. D., Rouzaud, F., Kikuchi, K., Tamaki, K. and Hearing, V. J. (2006). The repeat domain of the melanosomal matrix protein PMEL17/GP100 is required for the formation of organellar fibers. *J. Biol. Chem.* **281**, 21198-21208. doi:10.1074/jbc.M601643200
- Hoogdijn, M. J., Smit, N. P., Van Der Laarse, A., van Nieuwpoort, A. F., Wood, J. M. and Thody, A. J. (2003). Melanin has a role in Ca²⁺ homeostasis in human melanocytes. *Pigment Cell Res.* **16**, 127-132. doi:10.1034/j.1600-0749.2003.00018.x
- Ito, S. and Wakamatsu, K. (2011). Human hair melanins: what we have learned and have not learned from mouse coat color pigmentation. *Pigment Cell Melanoma Res.* **24**, 63-74. doi:10.1111/j.1755-148X.2010.00755.x
- Kiyoshima, D., Kawakami, K., Hayakawa, K., Tatsumi, H. and Sokabe, M. (2011). Force- and Ca²⁺-dependent internalization of integrins in cultured endothelial cells. *J. Cell Sci.* **124**, 3859-3870. doi:10.1242/jcs.088559
- Kostic, M., Ludtmann, M. H. R., Bading, H., Hershinkel, M., Steer, E., Chu, C. T., Abramov, A. Y. and Sekler, I. (2015). PKA Phosphorylation of NCLX reverses mitochondrial calcium overload and depolarization, promoting survival of PINK1-deficient dopaminergic neurons. *Cell Rep.* **13**, 376-386. doi:10.1016/j.celrep.2015.08.079
- Kushimoto, T., Basrur, V., Valencia, J., Matsunaga, J., Vieira, W. D., Ferrans, V. J., Muller, J., Appella, E. and Hearing, V. J. (2001). A model for melanosome biogenesis based on the purification and analysis of early melanosomes. *Proc. Natl. Acad. Sci. USA* **98**, 10698-10703. doi:10.1073/pnas.191184798
- Laddha, N. C., Dwivedi, M., Mansuri, M. S., Gani, A. R., Ansarullah, M., Ramachandran, A. V., Dalai, S. and Begum, R. (2013). Vitiligo: interplay between oxidative stress and immune system. *Exp. Dermatol.* **22**, 245-250. doi:10.1111/exd.12103
- Lamason, R. L., Mohideen, M. A., Mest, J. R., Wong, A. C., Norton, H. L., Aros, M. C., Juryneec, M. J., Mao, X., Humphreville, V. R., Humbert, J. E. et al. (2005). SLC24A5, a putative cation exchanger, affects pigmentation in zebrafish and humans. *Science* **310**, 1782-1786. doi:10.1126/science.1116238
- Li, W., He, M., Zhou, H., Bourne, J. W. and Liang, P. (2006). Mutational data integration in gene-oriented files of the Hermansky-Pudlak Syndrome database. *Hum. Mutat.* **27**, 402-407. doi:10.1002/humu.20309
- Luongo, T. S., Lambert, J. P., Gross, P., Nwokedi, M., Lombardi, A. A., Shanmughapriya, S., Carpenter, A. C., Kolmetzky, D., Gao, E., van Berlo, J. H. et al. (2017). The mitochondrial Na⁺/Ca²⁺ exchanger is essential for Ca²⁺ homeostasis and viability. *Nature* **545**, 93-97. doi:10.1038/nature22082
- Minta, A., Kao, J. P. and Tsien, R. Y. (1989). Fluorescent indicators for cytosolic calcium based on rhodamine and fluorescein chromophores. *J. Biol. Chem.* **264**, 8171-8178.
- Morice-Picard, F., Lasseaux, E., François, S., Simon, D., Rooryck, C., Bieth, E., Colin, E., Bonneau, D., Journal, H., Walraedt, S. et al. (2014). SLC24A5 mutations are associated with non-syndromic oculocutaneous albinism. *J. Invest. Dermatol.* **134**, 568-571. doi:10.1038/jid.2013.360
- Niel, G. V., Charrin, S., Simoes, S., Romao, M., Rochin, L., Saftig, P., Marks, M. S., Rubinstein, E. and Raposo, G. (2011). The tetraspanin CD63 regulates ESCRT-independent and -dependent endosomal sorting during melanogenesis. *Dev. Cell* **21**, 708-721. doi:10.1016/j.devcel.2011.08.019
- Palty, R., Silverman, W. F., Hershinkel, M., Caporale, T., Sensi, S. L., Parnis, J., Nolte, C., Fishman, D., Shoshan-Barmatz, V., Herrmann, S. et al. (2010). NCLX is an essential component of mitochondrial Na⁺/Ca²⁺ exchange. *Proc. Natl. Acad. Sci. U.S.A.* **107**, 436-441. doi:10.1073/pnas.0908099107
- Patel, S. and Docampo, R. (2010). Acidic calcium stores open for business: expanding the potential for intracellular Ca²⁺ signaling. *Trends Cell Biol.* **20**, 277-286. doi:10.1016/j.tcb.2010.02.003
- Puri, V., Watanabe, R., Singh, R. D., Dominguez, M., Brown, J. C., Wheatley, C. L., Marks, D. L. and Pagano, R. E. (2001). Clathrin-dependent and -independent internalization of plasma membrane sphingolipids initiates two Golgi targeting pathways. *J. Cell Biol.* **154**, 535-547. doi:10.1083/jcb.200102084
- Raposo, G., Tenza, D., Murphy, D. M., Berson, J. F. and Marks, M. S. (2001). Distinct protein sorting and localization to premelanosomes, melanosomes, and lysosomes in pigmented melanocytic cells. *J. Cell Biol.* **152**, 809-823. doi:10.1083/jcb.152.4.809
- Rizzuto, R., Pinton, P., Carrington, W., Fay, F. S., Fogarty, K. E., Lifshitz, L. M., Tuff, R. A. and Pozzan, T. (1998). Close contacts with the endoplasmic reticulum as determinants of mitochondrial Ca²⁺ responses. *Science* **280**, 1763-1766. doi:10.1126/science.280.5370.1763
- Rizzuto, R., Marchi, S., Bonora, M., Aguiari, P., Bononi, A., De Stefani, D., Giorgi, C., Leo, S., Rimessi, A., Siviero, R. et al. (2009). Ca²⁺ transfer from the ER to mitochondria: when, how and why. *Biochim. Biophys. Acta* **1787**, 1342-1351. doi:10.1016/j.bbabi.2009.03.015
- Rogasevskaia, T. P., Szerencsei, R. T., Jalloul, A. H., Visser, F., Winkfein, R. J. and Schnetkamp, P. P. M. (2019). Cellular localization of the K(+) -dependent Na(+) -Ca(2+) exchanger NCKX5 and the role of the cytoplasmic loop in its distribution in pigmented cells. *Pigment Cell Melanoma Res.* **32**, 55-67. doi:10.1111/pcmr.12723
- Schnetkamp, P. P. M. (2013). The SLC24 gene family of Na⁺/Ca²⁺-K⁺ exchangers: from sight and smell to memory consolidation and skin pigmentation. *Mol. Aspects Med.* **34**, 455-464. doi:10.1016/j.mam.2012.07.008
- Seiberg, M. (2013). Age-induced hair greying: the multiple effects of oxidative stress. *Int. J. Cosmet. Sci.* **35**, 532-538. doi:10.1111/ics.12090
- Shumilina, E., Xuan, N. T., Matzner, N., Bhandaru, M., Zemtsova, I. M. and Lang, F. (2010). Regulation of calcium signaling in dendritic cells by 1,25-dihydroxyvitamin D3. *FASEB J.* **24**, 1989-1996. doi:10.1096/fj.09-142265
- Sitaram, A. and Marks, M. S. (2012). Mechanisms of protein delivery to melanosomes in pigment cells. *Physiology (Bethesda)* **27**, 85-99. doi:10.1152/physiol.00043.2011
- Thomas, G. (2002). Furin at the cutting edge: from protein traffic to embryogenesis and disease. *Nat. Rev. Mol. Cell Biol.* **3**, 753-766. doi:10.1038/nrm934
- Vance, J. E. (1990). Phospholipid synthesis in a membrane fraction associated with mitochondria. *J. Biol. Chem.* **265**, 7248-7256.
- Wasmeier, C., Romao, M., Plowright, L., Bennett, D. C., Raposo, G. and Seabra, M. C. (2006). Rab38 and Rab32 control post-Golgi trafficking of melanogenic enzymes. *J. Cell Biol.* **175**, 271-281. doi:10.1083/jcb.200606050
- Wei, A.-H. and Li, W. (2013). Hermansky-Pudlak syndrome: pigmentary and non-pigmentary defects and their pathogenesis. *Pigment Cell Melanoma Res.* **26**, 176-192. doi:10.1111/pcmr.12051
- Wei, A.-H., Zang, D.-J., Zhang, Z., Liu, X.-Z., He, X., Yang, L., Wang, Y., Zhou, Z.-Y., Zhang, M.-R., Dai, L.-L. et al. (2013). Exome sequencing identifies SLC24A5 as a candidate gene for nonsyndromic oculocutaneous albinism. *J. Invest. Dermatol.* **133**, 1834-1840. doi:10.1038/jid.2013.49
- Yasumoto, K., Watabe, H., Valencia, J. C., Kushimoto, T., Kobayashi, T., Appella, E. and Hearing, V. J. (2004). Epitope mapping of the melanosomal matrix protein gp100 (PMEL17): rapid processing in the endoplasmic reticulum and glycosylation in the early Golgi compartment. *J. Biol. Chem.* **279**, 28330-28338. doi:10.1074/jbc.M401269200